Mixed-mode dynamic stress intensity factors evaluation using ordinary state-based peridynamics

Michiya Imachi[a], Satoyuki Tanaka[a], Tinh Quoc Bui[b]

[a] *Graduate School of Engineering, Hiroshima University, Japan, e-mail: d174722@hiroshima-u.ac.jp, satoyuki@hiroshima-u.ac.jp*
[b] *Department of Civil and Environmental Engineering, Tokyo Institute of Technology, Japan, e-mail: bui.t.aa@m.titech.ac.jp*

Abstract

Mixed-mode dynamic stress intensity factors (DSIFs) for two-dimensional (2D) elastic cracked solids are evaluated employing ordinary state-based peridynamics (OSPD) theory. The interaction integral is adopted in the evaluation of the DSIFs. Because the displacement derivative cannot be evaluated in the standard OSPD theory, the derivative components in the interaction integral are derived based on the moving least-squares approximation (MLSA). In addition, the diffraction method is introduced in the MLSA to accurately evaluate the field variables around the crack. Several 2D mixed-mode crack problems are solved and evaluated DISFs for regular and irregular particle arrangements. High accuracy and path-independent mixed-mode DSIFs are achieved by this present formulation and discretization.

Keywords: Fracture Mechanics, Peridynamics, Dynamic Stress Intensity Factors, Moving Least-Squares

1. Introduction

In the last two decades, meshfree Galerkin methods have been developed for modeling in science and engineering research fields, and in particular fracture problems. In the meshfree formulation and discretization, particles are distributed entire the analysis domain and meshfree interpolants are employed for each particle to approximate field variables. The equilibrium equation for a continuum is transformed into weak form and is discretized using the scattered particles. The point of note is that fracture modeling, specifically, the displacement discontinuity along crack segment and the representa-

tion of severe stress concentration around the crack-tip, is introduced via the meshfree discretization. To date, several meshfree and related methodologies have been proposed, *e.g.*, element-free Galerkin method [1], reproducing kernel particle method [2-4], moving Kriging interpolation-based meshfree method [5-8] and wavelet Galerkin method [9-14]. Although there are several advantages in solving fracture problems using meshfree methods compared with the finite element method (FEM), there remains several challenging problems in fracture modeling, *e.g.*, dynamic fracture, multiple cracks and fragmentation problems. Even when the problems are discretized by nodes or particles, Galerkin-based formulation sometime includes difficulties because it is formulated based on continuum mechanics theory.

A novel numerical method, *i.e.*, peridynamics (PD) theory, has recently been proposed by Silling [15] for analyzing solid mechanics problems. In the PD theory, the equation of motion is formulated and particles are scattered over the entire body in the discretization, as well as molecular dynamics theory. The equation of motion is not based on Galerkin formulation. Each particle has a function support "Horizon" and each particle within this Horizon is connected by a "Bond". Attractive pairwise forces interact over the particles to model a continuum like molecular dynamics theory. The prototype micro-brittle (PMB) model [16] is often adopted to model a brittle fracture in cracked solids. Fracture energy is defined and a bond across the crack segment is separated when the strain energy reaches a critical value. Therefore, because of simplicity in this fracture modeling, the PD theory is well suited for analyzing fracture problems, especially those that include branching, multiple cracks, and fragmentation. Various studies have employed PD theory for analyzing fracture in fibers [17] and membranes [18]. Crack branching problems in brittle material are analyzed in [19-22]. In addition, methods coupled with Galerkin-based approach [23-27] have also been presented.

The evaluation of fracture mechanics parameters, *e.g.*, dynamic stress intensity factors (DSIFs), is important in analyzing such fracture problems in solids. Fracture behaviors can be treated effectively based on classical fracture mechanics theory. Researchers have performed evaluations of fracture mechanics parameters for the PD theory [28-30]. However, accurate evaluations of the DSIFs of cracked solids in terms of the PD theory are rare. In the present study, mixed-mode DSIFs for two-dimensional (2D) elastic cracked solids are evaluated employing ordinary state-based PD (OSPD) theory of Le *et al.* [31]. The interaction integral is adopted to extract mixed-mode DSIFs

from the J-integral. Because the standard OSPD theory cannot directly be used to evaluate the displacement derivative, the moving least-squares approximation (MLSA) is therefore adopted for this purpose in the interaction integral. In addition, the diffraction method [32] is introduced in the MLSA to approximate physical values around the crack. Although elastodynamic problems and single-mode DSIF were evaluated in our previous study [33] to verify accuracy in 2D elastic continuum as well as examination of skin effect, mixed-mode problems have not been reported to date. The interaction integral method is adopted and implemented in the OSPD theory. The path-independent property and accuracy of the DSIFs are critically examined for several 2D mixed-mode crack problems.

The structure of the paper is organized as follows: OSPD theory is briefly described in Section 2. The interaction integral and numerical implementation in the OSPD theory are presented in Section 3. Several numerical examples and verification of mixed-mode DSIFs are analyzed and discussed in Section 4. Major conclusions drawn from the study are given in Section 5.

2. Peridynamics theory

2.1. Basic theory

PD is a non-local theory and is considered as an augmented theory of molecular dynamics for analyzing continuum mechanics problems. In the PD discretization, particles are interacting with each other within an influence radius δ, called the "Horizon". In the state-based PD theory [34], the equation of motion is represented for a unit volume,

$$\rho\ddot{\mathbf{u}}(\mathbf{x},t) = \int_{\mathcal{H}} \Big[\underline{\mathbf{T}}(\mathbf{x},t)\langle\mathbf{x}'-\mathbf{x}\rangle - \underline{\mathbf{T}}(\mathbf{x}',t)\langle\mathbf{x}-\mathbf{x}'\rangle\Big]\mathrm{d}V_{\mathbf{x}'} + \mathbf{b}(\mathbf{x},t), \tag{1}$$

where ρ, $\ddot{\mathbf{u}}(\mathbf{x},t)$, $\mathrm{d}V_{\mathbf{x}'}$ and $\mathbf{b}(\mathbf{x},t)$ denote the mass density, acceleration vector, unit volume, and body force density, respectively. $\mathbf{x}$ is the position vector of a reference particle and a superscript "$\prime$" signifies an arbitrary particle within a neighborhood $\mathcal{H}$ of particle $\mathbf{x}$. $\langle\mathbf{x}'-\mathbf{x}\rangle$ represents the interaction between particles $\mathbf{x}$ and $\mathbf{x}'$ and is called the "Bond". $\underline{\mathbf{T}}(\mathbf{x},t)\langle\mathbf{x}'-\mathbf{x}\rangle$ is not a multiplication of $\underline{\mathbf{T}}(\mathbf{x},t)$ and $\langle\mathbf{x}'-\mathbf{x}\rangle$, but $\underline{\mathbf{T}}(\mathbf{x},t)$ is a function of state $\langle\mathbf{x}'-\mathbf{x}\rangle$. $\underline{\mathbf{T}}(\mathbf{x},t)\langle\mathbf{x}'-\mathbf{x}\rangle$ is called "Force state" to represent the particles interaction between $\mathbf{x}$ and $\mathbf{x}'$ at time t. To simplify its representation, we rewrite $\underline{\mathbf{T}}(\mathbf{x},t)\langle\mathbf{x}'-\mathbf{x}\rangle$ and $\underline{\mathbf{T}}(\mathbf{x}',t)\langle\mathbf{x}-\mathbf{x}'\rangle$ as $\underline{\mathbf{T}}$ and $\underline{\mathbf{T}}'$, respectively. So far,

a force state $\underline{\mathbf{T}}$ is formulated by three types of model [34] as; 1) "Bond based model", 2) "Ordinary state-based model" and 3) "Non-ordinary state-based model", respectively. A bond based model can be adopted for Poisson's ratio $\nu = 1/3$ for 2D problem and $\nu = 1/4$ for 3D problem. In addition, it was reported that "zero-energy mode" problem occurs in a non-ordinary state-based model [29]. In present study, a ordinary state-based model is chosen.

2.2. 2D OSPD theory

Le *et al.* [31] proposed a novel PD formulation for analyzing the 2D plane stress/plane strain solid mechanics problems for OSPD theory. Here, the OSPD theory and Le's formulation are introduced briefly. For more details of the OSPD and this formulation, see [31,34].

A force state $\underline{\mathbf{T}}$ in Eq.(1) is derived based on the strain energy density function $\nabla W(\theta, \underline{e}^{\mathrm{d}})$. It is written

$$\underline{\mathbf{T}} = \nabla W(\theta, \underline{e}^{\mathrm{d}}) = \underline{t}\frac{\boldsymbol{\xi} + \boldsymbol{\eta}}{|\boldsymbol{\xi} + \boldsymbol{\eta}|}, \tag{2}$$

where $\nabla W(\theta, \underline{e}^{\mathrm{d}})$ is a function of the volume dilatation θ and deviatoric part of the extension state $\underline{e}^{\mathrm{d}}$. When Eq.(2) satisfies, the material is called "Ordinary material". $\underline{t}$ is a scalar function and $\boldsymbol{\xi} + \boldsymbol{\eta}/|\boldsymbol{\xi} + \boldsymbol{\eta}|$ is a unit vector of direction. The relative position vector $\boldsymbol{\xi}$ and the relative displacement vector $\boldsymbol{\eta}$ are respectively defined by

$$\begin{aligned} \boldsymbol{\xi} &= \mathbf{x}' - \mathbf{x}, \\ \boldsymbol{\eta} &= \mathbf{u}' - \mathbf{u}. \end{aligned} \tag{3}$$

The strain energy density function of the OSPD is then obtained using

$$W(\theta, \underline{e}^{\mathrm{d}}) = \frac{\kappa'}{2}\theta^2 + \frac{\alpha}{2}(\underline{\omega(\xi)}\underline{e}^{\mathrm{d}}) \bullet \underline{e}^{\mathrm{d}}, \tag{4}$$

where $\underline{\omega(\xi)}$ is an arbitrary influence function which depends on the distance between particles. A Gaussian function is chosen. κ' and α are determined from the constitutive law of the material. The dot product "$\bullet$" represents the domain of integration for arbitrary states within the neighborhood. For instance, the dot product of same order states $\underline{A}$ and $\underline{B}$ as defined by

$$\underline{A} \bullet \underline{B} = \int_{\mathcal{H}_{\mathbf{x}}} \underline{AB}\, \mathrm{d}V_{\mathbf{x}'}. \tag{5}$$

The volume dilation θ and the deviatoric part of the extension $\underline{e}^{\mathrm{d}}$ are defined by

$$\theta = \frac{3(\underline{\omega(\xi)}\underline{x}) \bullet \underline{e}}{(\underline{\omega(\xi)}\underline{x}) \bullet \underline{x}}, \tag{6}$$

$$\underline{e}^{\mathrm{d}} = \underline{e} - \frac{\theta}{3}\underline{x}, \tag{7}$$

where $\underline{x}=|\boldsymbol{\xi}|$ and $\underline{e}=|\boldsymbol{\xi}+\boldsymbol{\eta}|-|\boldsymbol{\xi}|$. The scalar function $\underline{t}$ in Eq.(2) for the plane stress condition is given by

$$\underline{t} = \frac{2(2\nu-1)}{\nu-1}\Big(\kappa'\theta - \frac{\alpha}{3}(\underline{\omega(\xi)}\underline{e}^{\mathrm{d}}) \bullet \underline{x}\Big)\frac{\underline{\omega(\xi)}\underline{x}}{(\underline{\omega(\xi)}\underline{x}) \bullet \underline{x}}, \tag{8}$$

$$\alpha = \frac{8G}{(\underline{\omega(\xi)}\underline{x}) \bullet \underline{x}} \quad , \quad \kappa' = K + \frac{G(\nu+1)^2}{9(2\nu-1)^2}, \tag{9}$$

and for the plane strain condition, by:

$$\underline{t} = 2\left(\kappa'\theta - \frac{\alpha}{3}\underline{\omega(\xi)}\underline{e}^{\mathrm{d}} \bullet \underline{x}\right)\frac{\underline{\omega(\xi)}\underline{x}}{(\underline{\omega(\xi)}\underline{x}) \bullet \underline{x}} + \alpha\underline{\omega(\xi)}\underline{e}^{\mathrm{d}}, \tag{10}$$

$$\alpha = \frac{8G}{(\underline{\omega(\xi)}\underline{x}) \bullet \underline{x}} \quad , \quad \kappa' = K + \frac{G}{9}, \tag{11}$$

where G and K are the elastic shear and bulk moduli, respectively. To evaluate stress components of the PD theory, a collapse stress tensor [35] is employed. The stress tensor is written

$$\boldsymbol{\sigma} = \int_{\mathcal{H}_{\mathbf{x}}} \underline{\mathbf{T}} \otimes \boldsymbol{\xi}\, \mathrm{d}V_{\mathbf{x}'}. \tag{12}$$

2.3. Crack modeling

In the PD model, the analysis domain is discretized using the scattered particles. Voronoi diagram [36] is employed to determine the initial volume of each particle. A crack is modeled by a pairwise forces of the distributed particles crossing the segment. When a crack segment intersects a bond, the bond is broken as shown in Fig.1. The solid lines mean bonds join a pair of particles and dashed lines represent broken bonds. When bonds are broken, the pairwise force of the force state in Eq.(1) become zero.

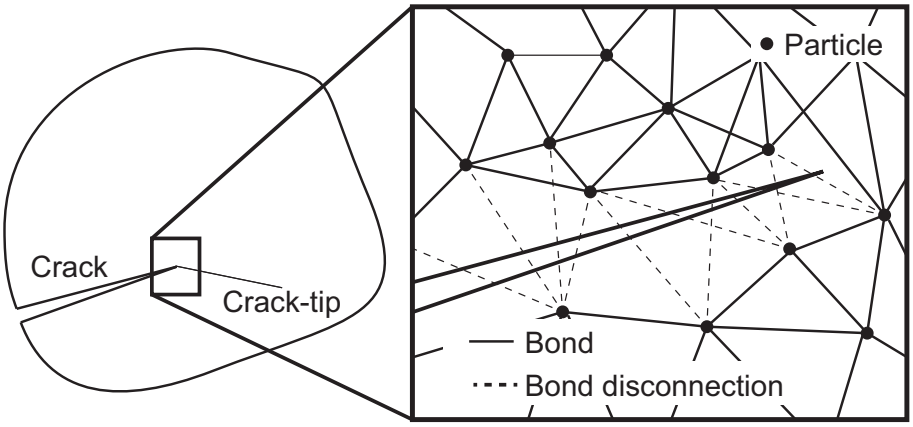

Figure 1: Schematic of crack modeling in a PD theory.

3. Evaluation of DSIFs

3.1. Interaction integral

The interaction integral [37] is adopted in extracting mixed-mode DSIFs from the J-integral [38] in the OSPD theory. The interaction integral is briefly described. Here, we consider two kinds of fields, *i.e.*, actual displacement fields u^{act} and auxiliary displacement fields u^{aux}. When considering an equivalent domain integral form of the J-integral under the superimposed state of actual-plus-auxiliary fields, the interaction integral I can be written

$$\begin{aligned} I = \int_{\Omega} \Big[\Big((\sigma_{ij}^{\text{act}} + \sigma_{ij}^{\text{aux}}) (\frac{\partial u_i}{\partial x_1}^{\text{act}} + \frac{\partial u_i}{\partial x_1}^{\text{aux}}) - \frac{1}{2} (\sigma_{ij}^{\text{act}} + \sigma_{ij}^{\text{aux}}) (\varepsilon_{ij}^{\text{act}} + \varepsilon_{ij}^{\text{aux}}) \delta_{1j} \Big) \frac{\partial q}{\partial x_j} \\ + \Big(\frac{\partial \sigma_{ij}}{\partial x_j}^{\text{act}} + \frac{\partial \sigma_{ij}}{\partial x_j}^{\text{aux}} \Big) \Big(\frac{\partial u_i}{\partial x_1}^{\text{act}} + \frac{\partial u_i}{\partial x_1}^{\text{aux}} \Big) q \Big] \mathrm{d}\Omega \\ = J^{\text{act}} + J^{\text{aux}} + M, \end{aligned} \tag{13}$$

where J^{act} and J^{aux} are the J-integrals with actual and auxiliary fields. The M corresponds to the interaction term of the actual and auxiliary states

(M-integral). It is written

$$M = \int_{\Omega} \Big[\Big(\sigma_{ij}^{\text{aux}} \frac{\partial u_i}{\partial x_1}^{\text{act}} + \sigma_{ij}^{\text{act}} \frac{\partial u_i}{\partial x_1}^{\text{aux}} - \frac{1}{2} (\sigma_{ij}^{\text{act}} \varepsilon_{ij}^{\text{aux}} + \sigma_{ij}^{\text{aux}} \varepsilon_{ij}^{\text{act}}) \delta_{1j} \Big) \frac{\partial q}{\partial x_j} + \Big(\frac{\partial \sigma_{ij}}{\partial x_j}^{\text{aux}} \frac{\partial u_i}{\partial x_1}^{\text{act}} + \frac{\partial \sigma_{ij}}{\partial x_j}^{\text{act}} \frac{\partial u_i}{\partial x_1}^{\text{aux}} \Big) q \Big] \mathrm{d}\Omega. \tag{14}$$

Note that, in linear fracture mechanics, Williams' solution [39] is adopted as the auxiliary field. The q-function is the arbitrary function satisfying conditions

$$q = \begin{cases} 0 & \text{outside of S2} \\ 1 & \text{inside of S1} \\ 0 \leq q \leq 1 & \text{otherwise} \end{cases}, \tag{15}$$

where S1 and S2 are domains that are defined near the crack-tip as shown in Fig.2(a). The linear function is chosen as the q-function. In Section 4, path-independence of the interaction integral is discussed using the q-functions with circular and rectangular forms as presented in Fig.2(b) and (c), respectively.

The relationship between the J-integrals and actual mixed-mode DSIFs K_{I} and K_{II} is written respectively as

$$J^{\text{act}} = \frac{(K_{\text{I}})^2 + (K_{\text{II}})^2}{E^*}, \tag{16}$$

$$J^{\text{aux}} = \frac{(K_{\text{I}}^{\text{aux}})^2 + (K_{\text{II}}^{\text{aux}})^2}{E^*}, \tag{17}$$

where

$$E^* = \begin{cases} E & \text{for plane stress} \\ E/(1-\nu^2) & \text{for plane strain} \end{cases}, \tag{18}$$

where $K_{\text{I}}^{\text{aux}}$ and $K_{\text{II}}^{\text{aux}}$ are the auxiliary mixed-mode DSIFs. Additionally, the interaction integral I is represented J-integral for the superimposed fields of actual and auxiliary, as follows

$$I = \frac{(K_{\text{I}}^{\text{act}} + K_{\text{I}}^{\text{aux}})^2 + (K_{\text{II}}^{\text{act}} + K_{\text{II}}^{\text{aux}})^2}{E^*}. \tag{19}$$

Substituting Eqs.(16), (17) and (19) into Eq.(13) leads to

$$M = \frac{K_{\mathrm{I}} K_{\mathrm{I}}^{\mathrm{aux}} + K_{\mathrm{II}} K_{\mathrm{II}}^{\mathrm{aux}}}{E^*}. \tag{20}$$

Consequently, the actual DSIFs of mode-I K_{I} and -II K_{II} can be obtained by assuming the pure mode-I ($K_{\mathrm{I}}^{\mathrm{aux}}$=1, $K_{\mathrm{II}}^{\mathrm{aux}}$=0) and -II ($K_{\mathrm{I}}^{\mathrm{aux}}$=0, $K_{\mathrm{II}}^{\mathrm{aux}}$=1) condition in the auxiliary fields, respectively; that is

$$K_{\mathrm{I}} = \frac{E^*}{2} M \qquad \text{for} \qquad K_{\mathrm{I}}^{\mathrm{aux}} = 1, \quad K_{\mathrm{II}}^{\mathrm{aux}} = 0, \tag{21}$$

$$K_{\mathrm{II}} = \frac{E^*}{2} M \qquad \text{for} \qquad K_{\mathrm{I}}^{\mathrm{aux}} = 0, \quad K_{\mathrm{II}}^{\mathrm{aux}} = 1. \tag{22}$$

3.2. Moving least-squares approximation

In the standard OSPD theory, the displacement gradient term in the M-integral of Eq.(14) cannot be defined explicitly, because the equation of motion can be evaluated without the displacement gradient. Therefore, an alternative way is required for the evaluation. The MLSA [40] is adopted. The approximation function $u^h(\mathbf{x})$ of an arbitrary function $u(\mathbf{x})$ is defined by

$$u^h(\mathbf{x}) = \sum_{i}^{m} p_i(\mathbf{x}) c_i(\mathbf{x}), \tag{23}$$

where $p_i(\mathbf{x})$ is a basis function, m is the number of basis function and $c_i(\mathbf{x})$ are the coefficients arising in the approximation. A quadratic basis $p_i(\mathbf{x}) = [1, x, y, x^2, xy, y^2]$ is taken as the basis function. The $c_i(\mathbf{x})$ can be determined by minimizing the weighted L_2-norm

$$Q = \sum_{I}^{N} w(\mathbf{x} - \mathbf{x}_I)[u^h(\mathbf{x}, \mathbf{x}_I) - u(\mathbf{x}_I)]^2. \tag{24}$$

Finally, the MLSA of function $u^h(\mathbf{x})$ can be given by

$$u^h(\mathbf{x}) = \sum_{I}^{N} \phi_I(\mathbf{x}) u(\mathbf{x}_I), \tag{25}$$

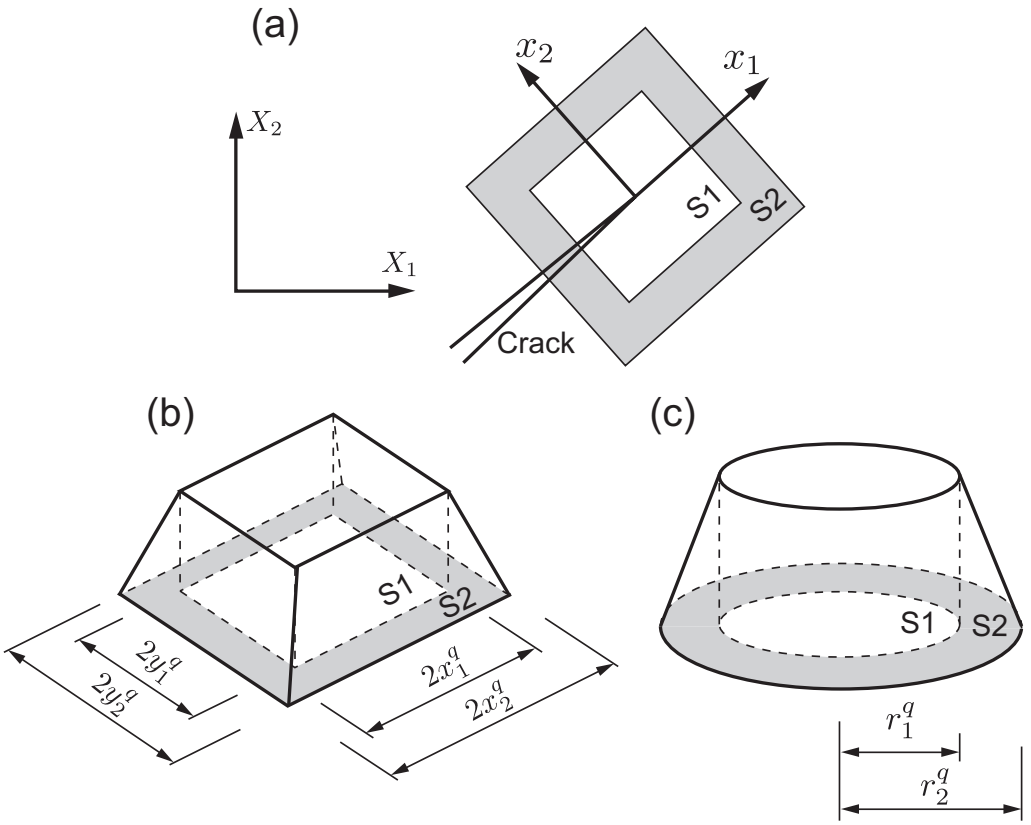

Figure 2: Geometry associated with the q-functions for the interaction integral (a) Global (X_1, X_2) and local (x_1, x_2) coordinate systems, (b) The rectangular q-function, (c) The circular q-function.

where N is the total number of particles within the neighborhood and $\phi_I(\mathbf{x})$ $(I = 1, \cdots, N)$ denote the shape functions. A cubic spline function is chosen as the weighted function $w(\mathbf{x} - \mathbf{x}_I)$ as follows:

$$w(\mathbf{x} - \mathbf{x}_i) = \frac{10}{7\pi\delta^2} \begin{cases} 1 - \frac{3}{2}s^2 + \frac{3}{4}s^3 & (0 \leq s \leq 1) \\ \frac{1}{4}(2-s)^3 & (1 \leq s \leq 2) \\ 0 & (2 \leq s) \end{cases}, \tag{26}$$

where s is the function dependent on the distance between paricles, as:

$$s = |\mathbf{x} - \mathbf{x}_i|/\delta. \tag{27}$$

The diffraction method [32] is also introduced to describe the near crack-tip precisely. This method is often used in providing the approximation function for the crack-tip continuity in the meshfree method [41-43].

3.3. Definition of the integration domain for the interaction integral

In using PD theory [21], the skin effect that particles along the boundary of the body generate inaccuracies may occur. To evaluate DSIFs with high accuracy employing the interaction integral, the effect near the crack-tip needs to treat consistently. Because Eq.(14) is domain integral form, error due to skin effect becomes large when domain of q-function is small. In the present study, to obtain high accuracy DSIFs, the domain for the q-function is defined larger than δ from the crack-tip as illustrated in Fig.3.

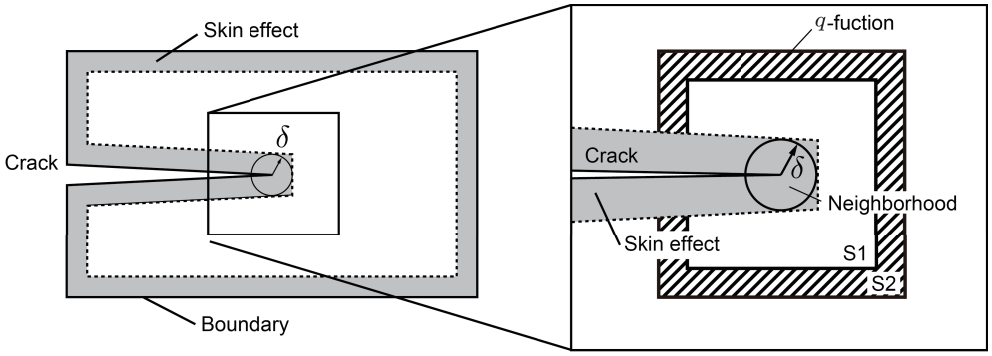

Figure 3: Skin effect and the definition of the q-function in the interaction integral.

4. Numerical results of mixed-mode DSIFs and discussion

With the central difference scheme adopted for the time integration, the acceleration $\ddot{\mathbf{u}}$ can be written

$$\ddot{\mathbf{u}}_i^n = \frac{\mathbf{u}_i^{n+1} - 2\mathbf{u}_i^n + \mathbf{u}_i^{n-1}}{\Delta t^2}, \tag{28}$$

where Δt is the time interval, and the superscript and subscript signify the time step and particle number, respectively. The equation of motion of Eq.(1) in discretization form becomes

$$\mathbf{u}_i^{n+1} = \frac{\Delta t^2}{\rho}\Big[\sum_j^{NP}(\underline{\mathbf{T}}_i^n - \underline{\mathbf{T}}_j^n)V_j + \mathbf{b}_i^n\Big] + 2\mathbf{u}_i^n - \mathbf{u}_i^{n-1}, \tag{29}$$

where $\underline{\mathbf{T}}_i^n$ is the force state of i-th particle at n-th step, V_j is the volume of j-th particle, $\mathbf{b}_j^n$ is the body force density of j-th particle at n-th step. NP is the total number of particles in the neighborhood. The Voronoi diagram is used to evaluate the volume of each particle as shown in Fig.4.

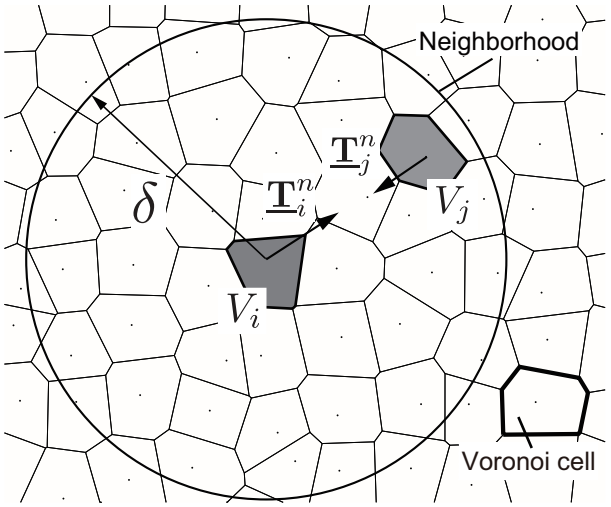

Figure 4: Schematic of the discretized PD model.

All numerical examples employ the normalized DSIFs,

$$\bar{K}_i^{\mathrm{dyn}} = K_i/\sigma_0\sqrt{\pi a}, \qquad (i = \mathrm{I}, \mathrm{II}) \tag{30}$$

where σ_0 is the magnitude of the applied stress for a cracked solid, and a is the crack length. In all numerical examples, plane strain conditions are assumed. All reference solutions were digitized for comparison. In our previous study [33], the numerical results in elastodynamics problems are converged sufficiently using a horizon δ that was larger than $3d$ in the 2D OSPD theory, where d is the particle distance. Hence, $\delta = 4d$ is chosen for all numerical examples. A very small time step Δt is chosen for the stable computations.

The DSIFs were examined by considering three numerical examples: an inclined cracked plate, an inclined cracked plate with a hole and a L-shaped plate with an inclined crack. The numerical results of the first example were compared with reference solutions and path-independence properties of the interaction integral were examined for different particle arrangements. In the second example, results from four different angle setting were examined. For the final example, an analysis of a complex L-shaped plate of general form was conducted.

4.1. An inclined cracked plate

An inclined crack in a rectangular plate with boundary condition in Fig.5 is analyzed. The geometry parameters are: width $B = 30$ mm, height $H = 60$ mm, crack length $2a = 14.14$ mm, angle of crack $\alpha = 45^\circ$. The plate has the following material properties: Young's modulus $E = 199.992$ GPa, Poisson's ratio $\nu = 0.3$ and mass density $\rho = 5,000$ kg/m^3. The particle distance $d = 0.05$ mm is used. The circular q-function in Fig.2(b) is chosen with radii of S1 $r_1^q = 1.2$ mm and S2 $r_2^q = 1.4$ mm.

A comparison of the normalized DSIFs with of Murti and Valliappan [44] and Fedelinski and Aliabadi [45] is shown in Fig.6. The DSIFs results in the present study shows a good agreement with the reference solutions.

In examining the path-independence of the interaction integral, the DSIFs were evaluated using the two types of arrangements, *i.e.*, regular and irregular particle settings as shown in Fig.7 for the three kinds of interaction integral domains. The irregular arrangement is modeled

$$\mathbf{x}_{\text{irr}} = \mathbf{x} + \Delta s \cdot r_c \cdot \beta_{\text{irr}}, \tag{31}$$

where $\mathbf{x}$ and $\mathbf{x}_{\text{irr}}$ are the position vectors for the regular and irregular arrangement, respectively. Δs is the particle distance and $\Delta s = d$ is used. r_c is a random factor, and an irregularity factor $\beta_{\text{irr}} = 0.3$ is used.

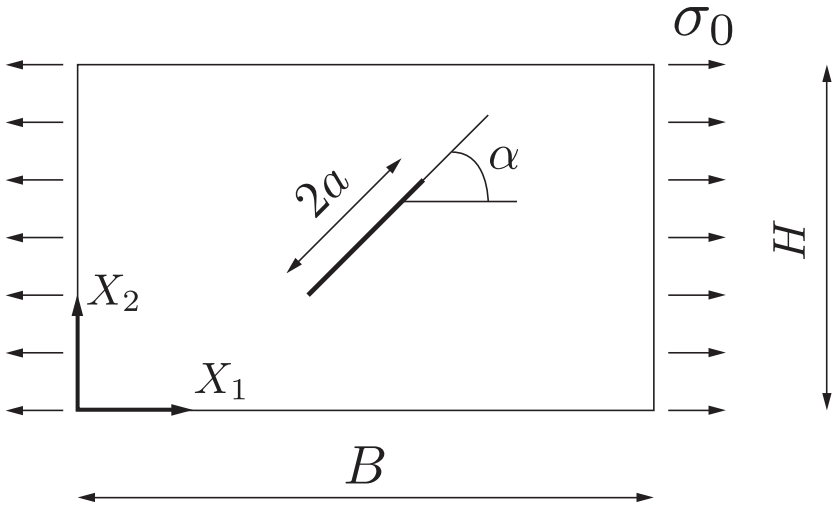

Figure 5: Rectangular plate with an inclined crack.

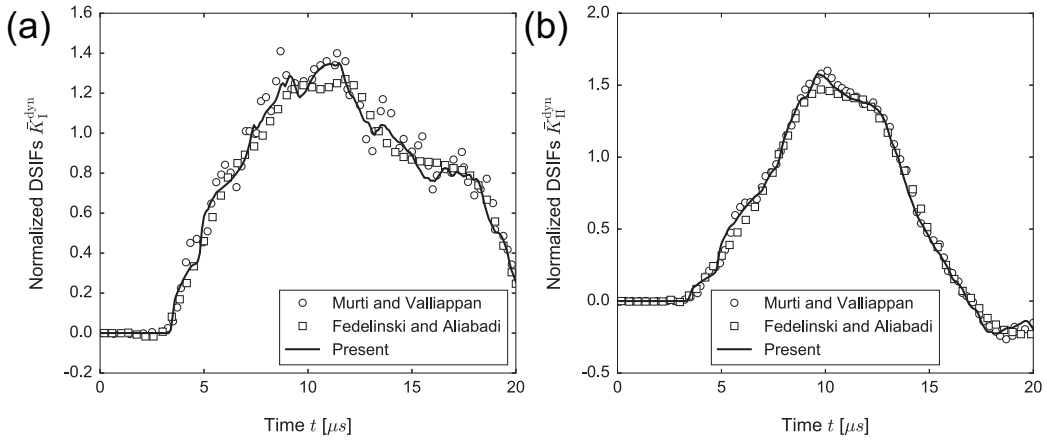

Figure 6: Comparison of the normalized DSIFs between the result of the present method and the reference solutions, (a) $\bar{K}_{\mathrm{I}}^{\mathrm{dyn}}$, (b) $\bar{K}_{\mathrm{II}}^{\mathrm{dyn}}$.

The properties of each domains are as follows: Domain A is circular, $r_1^q = 0.8$ mm and $r_2^q = 1.0$ mm: Domain B is circular, $r_1^q = 1.2$ mm and $r_2^q = 1.4$ mm: Domain C is rectangular, $x_1^q \times y_1^q = 1.5 \times 1.5$ mm and $x_2^q \times y_2^q = 1.7 \times 1.7$ mm. Comparisons between result for mode-I regular and irregular arrangements in Fig.8 (a) and (b) and for mode-II regular and irregular arrangements in Fig.8 (c) and (d) show that the respective DSIFs are in good agreement. More importantly, the present results exhibit path-independence implying that different domains do not significantly alter the DSIFs.

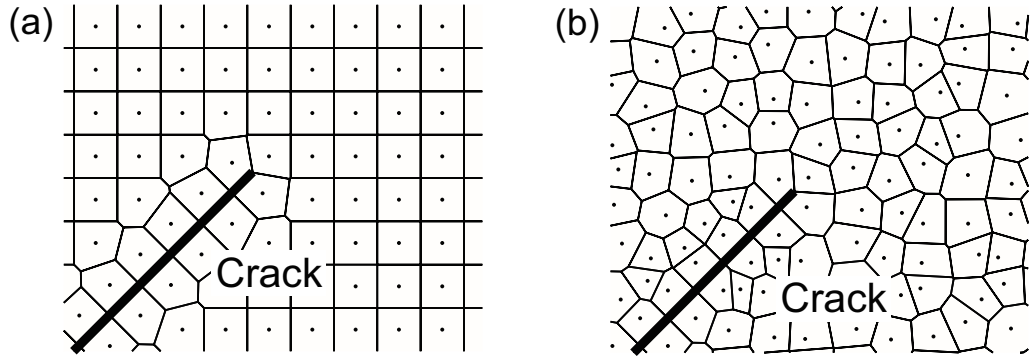

Figure 7: Arrangement of particles around the crack-tip, (a) regular arrangement, (b) irregular arrangement.

4.2. An inclined cracked plate with a hole

The next numerical example deals with an inclined cracked plate with a hole as shown in Fig.9. Boundary conditions are also depicted in the same figure. The crack length is $2a = 15$ mm. The plate width B and height H, also the material properties are taken same with the previous example. The DSIFs of this problem have been previously reported by Fedelinski and Aliabadi [45] using the dual boundary element method (dBEM), which are used here for our comparison purpose.

Four crack angles are considered and their corresponding DSIFs values are then analyzed. The particle distance $d = 0.075$ mm is used in this analysis. The circular q-function and the radius of S1 $r_1^q = 1.2$ mm and S2 $r_2^q = 1.5$ mm are used in all cases. A comparison between the results of the present method and the reference solutions is given in Fig.10.

For a crack angle $\alpha = 0^\circ$, the problem becomes pure mode-I: the DSIFs of mode-I take maximum values whereas the DSIFs of mode-II are zero. As

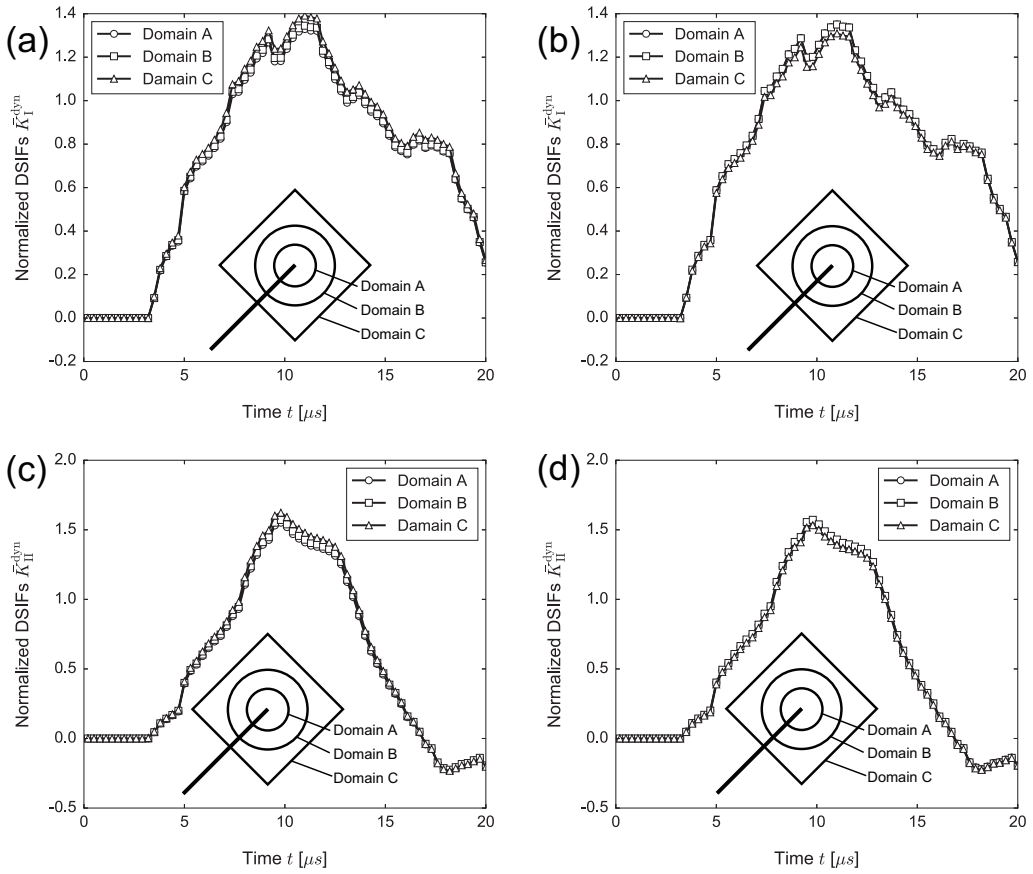

Figure 8: Path-independence for the interaction integral for the various arrangements (a) mode-I with regular arrangement, (b) mode-I irregular arrangement, (c) mode-II regular arrangement, (d) mode-II irregular arrangement.

the crack angle α increases, the DSIFs of mode-I decreases. The DSIFs of both modes are in good agreement with reference solutions.

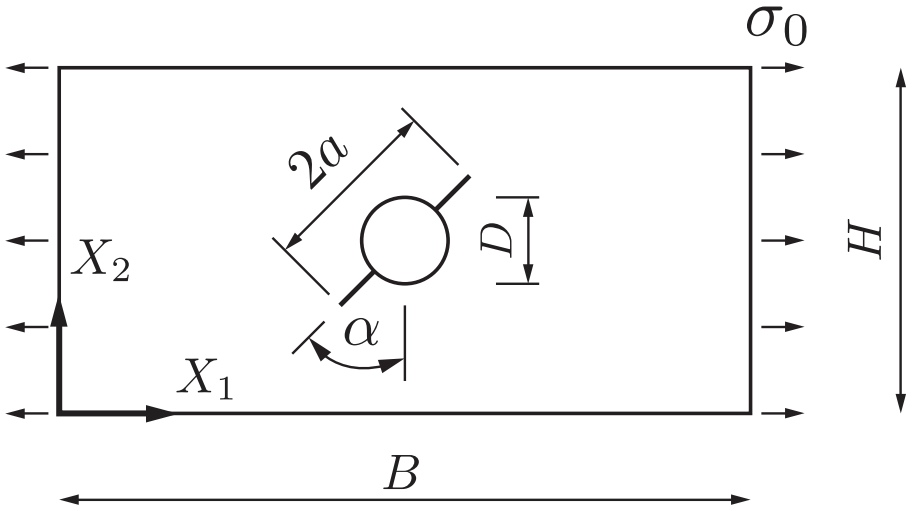

Figure 9: Inclined cracked plate with a hole.

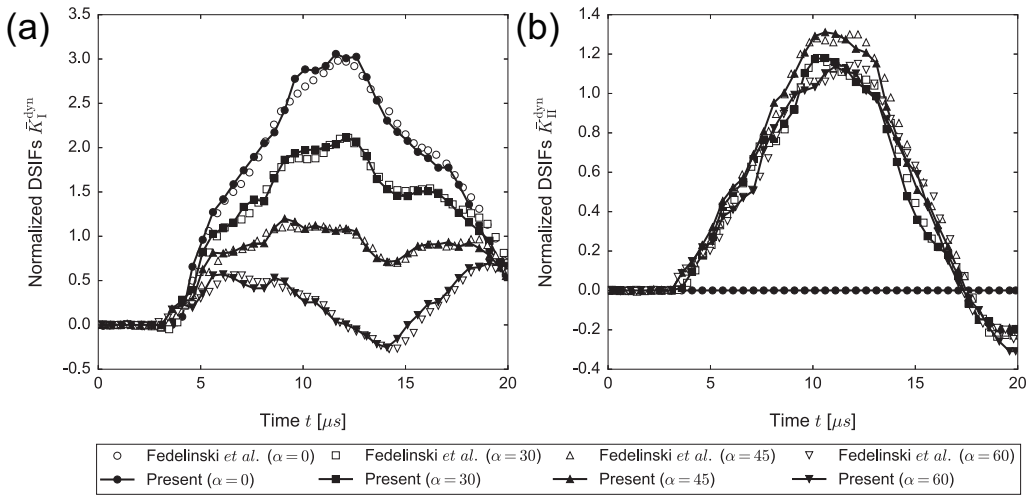

Figure 10: Comparison of normalized DSIFs between the results of the present method and the reference solutions for different crack angles ($\alpha = 0°,\ 30°,\ 45°,\ 60°$), (a) $\bar{K}_{\mathrm{I}}^{\mathrm{dyn}}$, (b) $\bar{K}_{\mathrm{II}}^{\mathrm{dyn}}$.

4.3. L-shaped plate with an inclined crack

The last numerical example is illustrates an analysis of DSIFs for a more complex configuration, a mixed-mode problem of an inclined crack in an L-shaped plate as shown in Fig.11(a). This model was solved by Fedelinski *et al.* [46] and their results used here for comparison purposes. The geometric parameters are settings: $B = 50$ mm, $H = 20$ mm, crack length $a = 10$ mm, angle of crack $\alpha = 45°$, and radius of curvature $R = 10$ mm. The material properties assumed are: Young's modulus $E = 200$ GPa, Poissson's ratio $\nu = 0.3$, mass density $\rho = 8,000$ kg/m^3. The particle distance $d = 0.1$ mm is used. The circular q-function with radii of S1 $r_1^q = 1.7$ mm and the radius of S2 $r_2^q = 2.1$ mm is used.

The numerical result of the normalized DSIFs are shown in Fig.11(b). As expected, the present DSIFs agree well with the reference solutions. As usual, the values of mode-I are larger than that of the mode-II. Whereas the more peaks are observed for the mode-I, no peak appears for the mode-II.

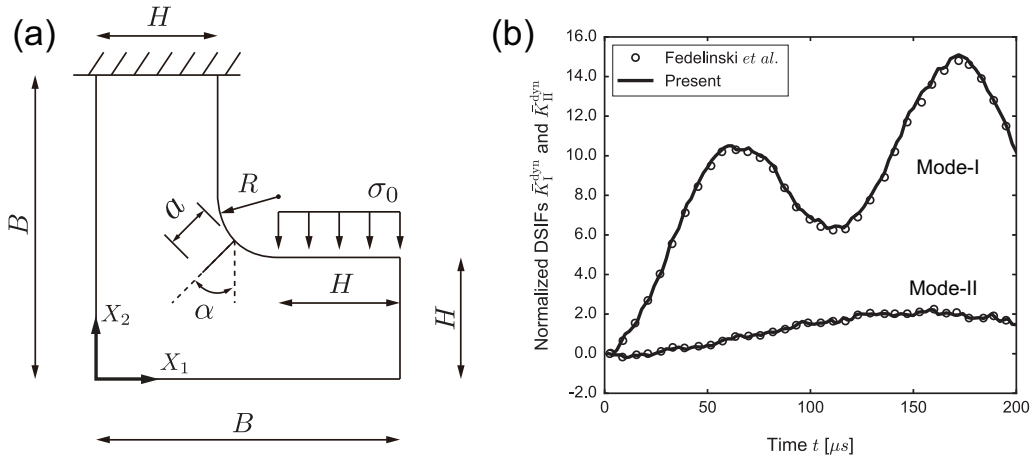

Figure 11: Inclined crack in an L-shaped plate, (a) the geometry and boundary conditions, (b) Comparison of DSIFs for mode-I and -II between result of the present method and reference solutions.

5. Conclusion

The mixed-mode DSIFs for the 2D plane problem with a stationary crack are evaluated using OSPD theory. The displacement gradient term in the interaction integral is calculated using the MLSA. To eliminate the skin effect

near the crack-tip, the region determining the influence of the q-function is set larger than δ. The accuracy of the present formulation was assessed using three numerical examples of mixed-mode problems that have reference solutions. The DSIFs of mixed-mode problems were evaluated employing both simple and sophisticated configurations. The present PD results yield good agreement with reference solutions based on boundary element method. In general, the developed PD approach offers high accuracy of the DSIFs and more importantly the path-independence of the DSIFs is obtained. The DSIFs evaluation can be adopted for dynamic crack propagation problems considering crack speed. The proposed approach is general and potentially to applicable to other complex fracture problems, for instance, multiphase smart piezoelectric materials [47].

Acknowledgements

This research was supported in part by Iwatani Naoji Foundation and the JSPS Grants-in-Aid for Young Scientists (B)(16K18323).

References

[1] T. Belytschko, Y.Y. Liu, L. Gu, Element-free Galerkin methods, Int. J. Numer. Meth. Eng. 37 (1994) 229-256.

[2] W.K. Liu, S. Jun, Y.F. Zhang, Reproducing kernel particle methods, Int. J. Numer. Meth. Fluid. 20 (1995) 1081-1106.

[3] S. Tanaka, S. Sadamoto, S. Okazawa, Nonlinear thin-plate bending analyses using the Hermite reproducing kernel approximation, Int. J. Comput. Meth. 9 (2012) 1240012.

[4] S. Sadamoto, S. Tanaka, S. Okazawa, Elastic large deflection analysis of plates subjected to uniaxial thrust using meshfree Mindlin-Reissner formulation, Comput. Mech. 52 (2013) 1313-1330.

[5] L. Gu, Moving Kriging interpolation and element-free Galerkin method, Int. J. Numer. Meth. Eng. 56 (2003) 1-11.

[6] T.Q. Bui, T.N. Nguyen, H. Nguyen-Dang, A moving Kriging interpolation-based meshless method for numerical simulation of Kirchhoff plate problems, Int. J. Numer. Meth. Eng. 77 (2009) 1371-1395.

[7] T.Q. Bui, M.N. Nguyen, A moving Kriging interpolation-based meshfree method for free vibration analysis of Kirchhoff plates, Comput. Struct. 89 (2011) 380-394.

[8] T.Q. Bui, M.N. Nguyen, C. Zhang, A moving Kriging interpolation-based element-free Galerkin method for structural dynamic analysis, Comput. Meth. Appl. Meth. Eng. 200 (2011) 1354-1366.

[9] K. Amaratunga, J.R. Williams, S. Quan, J. Weiss, Wavelet-Galerkin solutions for one-dimensional partial differential equations, Int. J. Numer. Meth. Eng. 37 (1994) 2703-2716.

[10] S. Tanaka, H. Okada, S. Okazawa, A wavelet Galerkin method employing B-spline bases for solid mechanics problems without the use of a fictitious domain, Comput. Mech. 50 (2012) 35-48.

[11] S. Tanaka, H. Okada, S. Okazawa, M. Fujikubo, Fracture mechanics analysis using the wavelet Galerkin method and extended finite element method, Int. J. Numer. Meth. Eng. 93 (2013) 1082-1108.

[12] S. Tanaka, H. Suzuki, S. Ueda, S. Sannomaru, An extended wavelet Galerkin method with a high-order B-spline for 2D crack problems, Acta. Mech. 226 (2015) 2159-2175.

[13] S. Tanaka, S. Sannomaru, M. Imachi, S. Hagihara, S. Okazawa, H. Okada, Analysis of dynamic stress concentration problems employing spline-based wavelet Galerkin method, Eng. Anal. Bound. Elem. 58 (2015) 129-139.

[14] S. Sannomaru, S. Tanaka, K. Yoshida, T.Q. Bui, S. Okazawa, S. Hagihara, Treatment of Dirichlet-type boundary conditions in the spline-based wavelet Galerkin method employing multiple point constraints, Appl. Math. Model. 43 (2017) 592-610.

[15] S.A. Silling, Reformulation of elasticity theory for discontinuities and long-range forces, J. Mech. Phys. Solid. 48 (2000) 175-209.

[16] S.A. Silling, E. Askari, A meshfree method based on the peridynamic model of solid mechanics, Comput. Struct. 83 (2005) 1526-1535.

[17] F. Bobaru, S.A. Silling, Peridynamic 3d models of nanofiber networks and carbon nanotube-reinforced composites, AIP Conference Proceedings 712 (2004) 1565-1570.

[18] S.A. Silling, F. Bobaru, Peridynamic modeling of membranes and fibers, Int. J. Non. Lin. Mech. 40 (2005) 395-409.

[19] B. Kilic, E. Madenci, Prediction of crack paths in a quenched glass plate by using peridynamic theory, Int. J. Fract. 156 (2009) 165-177.

[20] Y.D. Ha, F. Bobaru, Studies of dynamic crack propagation and crack branching with peridynamics, Int. J. Fract. 162 (2010) 229-244.

[21] Y.D. Ha, F. Bobaru, Characteristics of dynamic brittle fracture captured with peridynamics, Eng. Fract. Mech. 78 (2011) 1156-1168.

[22] A. Agwai, I. Guven, E. Madenci, Predicting crack propagation with peridynamics: a comparative study, Int. J. Fract. 171 (2011) 65-78.

[23] R.W. Macek, S.A. Siiling, Peridynamics via finite element analysis, Finite. Elem. Anal. Des. 43 (2007) 1169-1178.

[24] B. Kilic, E. Madenci, Coupling of peridynamic theory and the finite element method, J. Mech. Mater. Struct. 5 (2010) 707-733.

[25] C.T. Wu, Kiniematic constraints in the state-based peridynamics with mixed local/nonlocal gradient approximations, Comput. Mech. 54 (2014) 1255-1267.

[26] C.T. Wu, B. Ren, A stabilized non-ordinary state-based peridynamics for the nonlocal ductile material failure analysis in metal machining process, Comput. Meth. Appl. Mech. Eng. 291 (2015) 197-215.

[27] B. Ren, C.T. Wu, E. Askari, A 3D discontinuous Galerkin finite element method with the bond-based peridynamics model for dynamic brittle failure analysis, Int. J. Impact. Eng. 99 (2017) 14-25.

[28] W. Hu, Y.D. Ha, F. Bobaru, S.A. Silling, The formulation and computation of the nonlocal J-integral in bond-based peridynamics, Int. J. Fract. 176 (2012) 195-206.

[29] M.S. Breitenfeld, P.H. Geubelle, O. Weckner, S.A. Silling, Non-ordinary state-based peridynamic analysis of stationary crack problems, Comput. Meth. Appl. Mech. Eng. 272 (2014) 233-250.

[30] R. Panchadhara, P.A. Gordon, Application of peridynamic stress intensity factors to dynamic fracture initiation and propagation, Int. J. Fract. 201 (2016) 81-96.

[31] Q.V. Le, W.K. Chan, J. Schwartz, A two-dimensional ordinary, state-based peridynamic model for linearly elastic solids, Int. J. Numer. Meth. Eng. 98 (2014) 547-561.

[32] D. Organ, M. Fleming, T. Terry, T. Belytschko, Continuous meshless approximations for nonconvex bodies by diffraction and transparency, Comput. Mech. 18 (1996) 225-235.

[33] M. Imachi, S. Tanaka, Dynamics stress intensity factors evaluation employing ordinary state-based peridynamics, Trans. JSCES, 2016 (2016) 20160017. (in Japanese)

[34] S.A. Silling, M. Epton, O. Weckner, J. Xu, E. Askari, Peridynamic states and constitutive modeling, J. Elasticity. 88 (2007) 151-184.

[35] S.A. Silling, R.B. Lehoucq, Convergence of peridynamics to classical elasticity theory, J. Elasticity. 93 (2008) 13-37.

[36] http://www.qhull.org/ [accessed 10.1.17].

[37] F.H.K. Chen, R.T. Shield, Conservation laws in elasticity of the J-integral type, J. Appl. Math. Phys. 28 (1977) 1-22.

[38] J.R. Rice, A path independent integral and the approximate analysis of strain concentration by notches and cracks, J. Appl. Mech. 35 (1968) 379-386.

[39] M.L. Williams, On the stress distribution at the base of a stationary crack, J. Appl. Mech. 24 (1956) 109-114.

[40] P. Lancaster, K. Salkauskas, Surfaces generated by moving least squares methods, Math. Comput. 37 (1981) 141-158.

[41] M. Fleming, Y.A. Chu, B. Moran, T. Belytschko, Enriched element-free Galerkin methods for crack tip fields, Int. J. Numer. Meth. Eng. 40 (1997) 1483-1504.

[42] S. Tanaka, S. Suzuki, S. Sadamoto, M. Imachi, T.Q. Bui, Analysis of cracked shear deformable plates by an effective meshfree plate formulation, Eng. Fract. Mech. 144 (2015) 142-157.

[43] S. Tanaka, H. Suzuki, S. Sadamoto, S. Sannomaru, T.T. Yu, Q.T. Bui, J-integral evaluation for 2D mixed-mode crack problems employing a meshfree stabilized conforming nodal integration method, Comput. Mech. 58 (2016) 185-198.

[44] V. Murti, S. Valliappan, The use of quarter point elemtnt in dynamic crack analysis, Eng. Fract. Mech. 23 (1986) 585-614.

[45] P. Fedelinski, M.H. Aliabadi, D.P. Rooke, The dual boundary element method: $\hat{J}$-integral for dynamic stress intensity factors, Int. J. Fract. 65 (1994) 369-381.

[46] P. Fedelinski, M.H. Aliabadi, D.P. Rooke, The laplace transform DBEM for mixed-mode dynamic crack analysis, Comput. Struct. 59 (1996) 1021-1031.

[47] Q.T. Bui, Extended isogeometric dynamic and static fracture analysis for cracks in piezoelectric materials using NURBS, Comput. Meth. Appl. Mech. Eng. 295 (2015) 470-509.